Dynamic consolidation of superhard materials

Wenbo Yang
Lindhurst Laboratory of Experimental Geophysics, Seismological Laboratory, California Institute of Technology, Pasadena, California 91125

G. M. Bond
Department of Materials and Metallurgical Engineering, New Mexico Institute of Mining and Technology, Socorro, New Mexico 87801

Hua Tan
Beijing Institute of Technology, P. O. Box 327, Beijing, People's Republic of China

Thomas J. Ahrens
Lindhurst Laboratory of Experimental Geophysics, Seismological Laboratory, California Institute of Technology, Pasadena, California 91125

G. Liu
Department of Materials and Metallurgical Engineering, New Mexico Institute of Mining and Technology, Socorro, New Mexico 87801

(Received 20 May 1990; accepted 27 January 1992)

Shock consolidation experiments were conducted via flyer impact on synthetic diamond (6–12 μm) and cubic boron nitride (c-BN) (4–8 μm) admixed with SiC whisker (SCW), Si_3N_4 whisker (SNW), SiC powder, and Si powder contained in stainless steel capsules under the shock pressure range of 10–30 GPa. Scanning electron microscopy and transmission electron microscopy imaging of the samples revealed no plastic deformation or melting of diamond and virtually no deformation of c-BN, whereas the SCW and SNW were extensively melted and recrystallized into bundle-shaped crystallites. In contrast, SiC powder mixed with diamond was also melted but demonstrated equant grain growth. A new method to calculate the shock temperature and melt fraction is formulated on the basis of Miłewski's sphere-rod packing data. The new method assigns excess bulk volume to the zone around whiskers and yields a better description of the energy deposition mechanism of the consolidation of powder-whisker systems. Some of the experiments employed Sawaoka's post-shock annealing technique, in which the sample is sandwiched between two layers of a mixture of titanium powder plus carbon. Very well consolidated samples were obtained with post-shock heating under shock pressures of only about 11 GPa. Micro-Vickers hardness values up to 27 GPa were obtained for c-BN plus SCW at a low impact velocity of 1.45 km/s with post-shock heating. This hardness is similar to that obtained at a higher impact velocity of 1.95 km/s without post-shock heating. To understand the post-shock heating process, one-dimensional time dependent temperature profile calculations were conducted for the sample and Ti + C layers. Post-shock heating appears to be very important in the consolidation of powder and whisker admixture. The calculated optimum Ti + C thickness is about 0.8–1.7 mm at a porosity of 40% for a typical sample thickness of 2 mm. The heating and cooling time is a few milliseconds. Good compacts with micro-Vickers hardness values up to 28 GPa were also obtained upon shock consolidation of diamond plus Si admixtures.

I. INTRODUCTION

Dynamic consolidation of such superhard materials as diamond and (diamond-structured) cubic boron nitride (c-BN) initially in powder form with grain sizes in the range of 10–50 μm shows some promise as a potential process for obtaining large quantities of technologically useful compacts. Single crystal powders of diamond are available from natural and synthetic sources,[1] whereas c-BN single crystal powders are produced for abrasive applications with static high-pressure techniques.[2] Recently several studies have been conducted in which single crystal powders, initially in the range of 60–70% of crystal density, have been consolidated to nearly crystal density by driving initial shocks of amplitudes in the range of 30 GPa into sample containers within steel recovery fixtures. These shock pressures have been generated with both the impact of flyer plates accelerated with propellant and high explosive systems.[3,4] In the

case of diamond, scanning electron microscopy (SEM) images indicated that shock-induced interparticle bonding appears to result from local melting. Interparticle sliding upon compaction is suggested to produce this melting. Transmission electron microscopy (TEM) of shock consolidated diamond[5] demonstrates that this apparently melted material transforms, in part, to very fine polycrystalline diamond, an amorphous carbon phase, and graphite upon unloading and cooling. The presence of the graphite phase probably prevents this material from demonstrating exceptional small-scale strength in Vickers hardness tests. In contrast, single crystal c-BN compaction[6] requires considerably higher shock pressures (33–77 GPa) to consolidate to nearly crystal density. This material demonstrates an impressive hardness of 50 GPa approaching that of single crystal c-BN (66–75 GPa). The consolidation mechanism in these experiments is not known although surface melting may also be occurring. Because of the irregularity and brittleness of the single crystals used in shock loading experiments, sound bonding between grains is not easy to obtain as the crystals tend to crack rather than change their shape plastically to fill the space between them.

Recently, Tan and Ahrens[7] reported the c-BN admixed with either Si_3N_4 (SNW) or SiC (SCW) whiskers formed hard uniform compacts upon shock compression to 22–23 GPa, starting with mixtures that were ~70% of crystal density and contained 15 to 20% of whisker materials. Micro-Vickers hardness values as high as 50 GPa were obtained for c-BN plus SNW mixture.

In the present study this work is extended to include studies of shock consolidation of diamond admixtures with SNW, SCW, SiC powder, and Si powder. Samples were examined with SEM. In addition, a limited number of samples were studied by TEM. The TEM studies provided insight into the physics of consolidation mechanism of whisker-cubic crystal mixtures and motivated a modification of previous thermodynamic modeling methodology for shock consolidation. A new calculation model of consolidation of cubic crystal-whisker mixtures is presented and a series of revised thermodynamic calculations of the shock states achieved in the cubic crystal and whisker phases are conducted with this formulation. Finally, since many of our experiments employed layers of Ti + C surrounding our samples (first suggested by Sawaoka *et al.*, 1988), we have developed a thermal model to describe the post-shock thermal annealing that takes place in the assembly.

II. EXPERIMENTAL METHOD

In addition to the SCW, c-BN, and SNW used in previous experiments,[7] we employed β–SiC single crystal powder and Si single crystal powder. The β–SiC single crystal powder is a product of Ibiden Co. Ltd. This material is reported by the manufacturer to have an average crystal diameter of 0.28 μm. The main impurities, with a total mass of less than 1%, are Al, Fe, SiO_2, C, and H_2O. The Si powder is commercially obtained with sizes of –325 mesh (less than 44 μm). The impurities are also less than 1 wt.%.

Two series of new experiments were conducted. The first series of experiments, which we carried out with a 20 mm propellant gun, included diamond powder mixed with SCW, SNW, SiC powder, or Si powder in different mass ratios and initial porosities. Samples of pure diamond and SCW were also shock compressed to provide a comparison to the admixtures. The second series of experiments was conducted with a 40 mm propellant gun. In these experiments, following the idea of Sawaoka,[8] we consolidated the diamond (or c-BN) and SCW mixtures initially 2–3 mm thick, which were sandwiched by a 0.8–1.5 mm thick titanium and carbon black mixture. The purpose of the metallic titanium-carbon mixture is to provide a post-shock heat source to anneal the sample. The thermodynamics of this reaction and resultant heat flow are described in Sec. VI.

The sample was pressed into a stainless steel capsule and under a vacuum of about 30 μm. A tantalum flyer plate was used to impact the sample assembly. The thicknesses of these plates for the 20 mm gun and 40 mm gun were 1.5 mm and 2.6 mm, respectively. The recovery method with momentum trap techniques, as previously described,[7] was used.

III. RESULTS

A. Diamond powder plus SNW

Our results are summarized in Table I. The estimated shock pressures in these experiments are about 25 GPa. Of the five shots, four sample assemblies exploded, leaving a hole in the center of the recovered Ta flyer plate. We infer that these explosions result from the expansion of N_2 gas produced by the reaction

$$3C + Si_3N_4 = 3SiC + 2N_2$$

At ambient pressure and temperatures higher than 1626 K, the calculated Gibbs formation energy difference, ΔG, has negative values (Fig. 1). The Gibbs formation energy at high temperature of SiC and Si_3N_4 is obtained from Ref. 9, and the Gibbs formation energy of diamond is from Ref. 30. According to our new calculation method, the SNW in these experiments will have a post-shock temperature of 2173 K (melting point) and about 80% of them will be shock melted.

The SEM image of a sample piece recovered from shot 961 is shown in Fig. 2. It demonstrates that the SNW has melted but does not indicate strong bonding between diamond particles although good consolidation can be seen in the very well mixed region. The fracture

TABLE I. Diamond plus silicon nitride whisker (SNW) shock consolidation experiments.

Experiments

Shot no.	Mass fraction (%) Diamond	Mass fraction (%) SNW	Initial density (%)	Flyer velocity (km/s)	Recovered results
953	84	16	65	1.93	Compacted, almost exploded
961	84	16	70	1.95	Exploded, only a small piece recovered
962	80	20	66.6	1.97	Friable
968	84	16	65.5	1.96	Exploded
971	84	16	60	1.90 (s.s.304)	Exploded

Calculations

Shot no.	Initial density (%) Diamond	Initial density (%) SNW	P_H (GPa)	T_H (K) Diamond	T_H (K) SNW	T_p (K) Diamond	T_p (K) SNW	L (%) Diamond	L (%) SNW
953	67.1	56.8	22.2	1351	2173	1339	2173	9.2	81.9
961	72.2	61.1	25.6	1274	2173	1261	2173	8.3	79.1

of individual diamond crystals can be seen clearly. A better consolidated sample might have been obtained if the content of SNW had been increased and the sample had been consolidated under a lower pressure.

B. Diamond plus SCW

Most samples from these experiments were successfully recovered (Table II). Two rather hard samples were obtained from shots 969 and 973 with 20 and 25 wt.% SCW, respectively. A very well consolidated sample was obtained from shot 1028 (Fig. 3). For this shot, we added 30 wt.% SCW to the diamond powder and expected that the additional SCW would protect the diamond grains from being fractured. This shot provided the best compact achieved with diamond. However, the SEM images show that the diamond in all the present experiments is seriously fractured. Although the fusion bonding between diamond particles in some shots appears to be incomplete, the SEM images show that the SCW material is completely shock melted in all the experiments. In order to determine whether the Al_2O_3 shim was critical to the achievement of high quality compacts, we conducted shot 1007 (Table II) without an Al_2O_3 shim at the impact end of the sample. No evidence of consolidation was obtained from the SEM image for this experiment. The lack of consolidation is thought to result from the metallic spray from the sample container which contaminates the diamond plus SCW sample.

Although the fusion bonding between diamond particles in some shots appears to be incomplete, the SEM images indicate that the SCW material is completely shock melted and has flowed between the diamond particles.

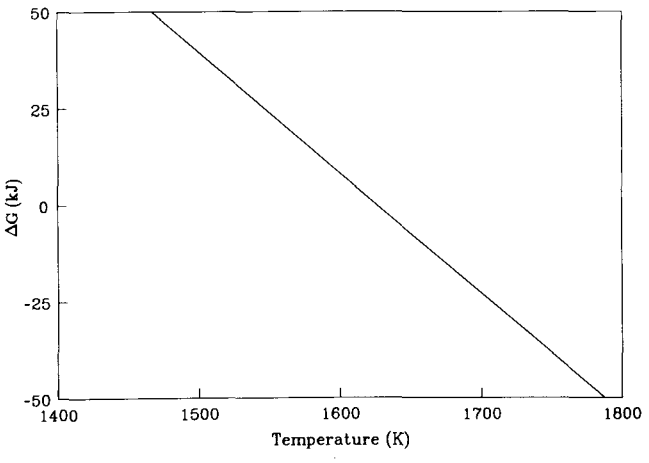

FIG. 1. Calculated Gibbs formation energy difference ΔG vs temperature of the reaction $3C + Si_3N_4 \rightarrow 3SiC + 2N_2\uparrow$.

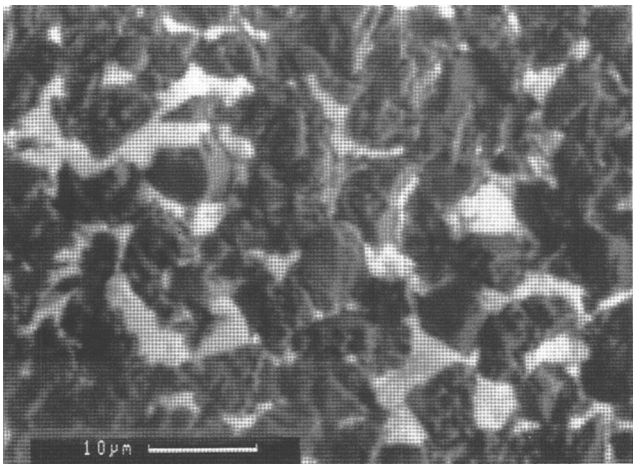

FIG. 2. SEM image of diamond plus SNW. Shot 961. The light-colored phase is silicon nitride whisker (SNW).

TABLE II. Diamond plus silicon carbide whisker (SCW) shock consolidation experiments.

Experiments

Shot no.	Mass fraction (%) Diamond	SCW	Initial density (%)	Flyer velocity (km/s)	Recovered results
966	80	20	70	1.99	Friable
969	80	20	60	1.90	Compacted, hardness ~ steel, cracks
970	100		55	1.90 (s.s.304)	Friable
973	75	25	60	2.00	Consolidated, hardness ~ WC, numerous cracks
1007	75	25	60	1.85	Uncompacted
1028	70	30	60	1.95	Consolidated, scratches sapphire

Calculations

Shot no.	Initial density % Diamond	SCW	P_H (GPa)	T_H (K) Diamond	SCW	T_p (K) Diamond	SCW	L (%) Diamond	SCW
969	63.7	49.7	19.0	1344	2953	1335	2894	9.1	37.7
973	66.8	47.0	20.7	1304	2963	1294	2963	8.7	45.8
1028	71.4	44.8	19.7	1117	2963	1109	2963	6.6	47.7

C. Diamond plus SiC powder and c-BN plus SiC powder

Unlike our previous results for shock compaction of c-BN plus SCW, no consolidated sample of c-BN plus SiC powder mixture was obtained. The major results are listed in Table III.

Diamond plus SiC powder also does not consolidate with the present method and the results are considerably less successful than the diamond plus SCW experiments.

D. Diamond plus SCW sandwiched with Ti + C

These experiments were conducted with a 40 mm gun rather than a 20 mm gun and employed samples that contained three layers: Ti plus C, diamond plus SCW, and Ti plus C. We chose a stoichiometric ratio for Ti to C equal to that in TiC of 3.99 to 1. The major results of the experiments are presented in Table IV. Notably, the impact velocity of the 2.6 mm thick Ta flyer plate is much lower than those used in 20 mm gun experiments (see Table II) and a longer shock duration is employed. The recovered samples indicated a well-consolidated appearance with very few cracks. Micro-Vickers hardness tests were conducted and resulted in a hardness of about 10 GPa. SEM images (Fig. 4) demonstrate that the whisker materials are not very well dispersed in the diamond powder and there are cracks in the SCW-rich zones. Moreover, the diamond powders, although well consolidated in what appears to be melted SCW, are unexpectedly severely cracked. Both the lack of ideal diamond-SCW dispersion and excessive diamond cracking probably interfere with obtaining optimum consolidation.

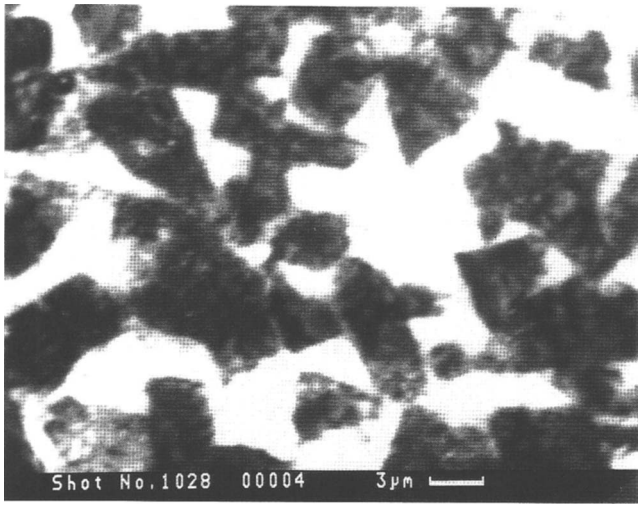

FIG. 3. SEM image of diamond plus SCW. Shot 1028 (SCW, light-colored phase) shows very well consolidated features. The fractures of diamond (dark phase) grains can be clearly seen in the image.

E. c-BN plus SCW sandwiched with Ti + C

Two shots were fired and the results are listed in Table V. The Ti + C layer is ~0.8 mm thick and the impact velocity is 1.35 to 1.45 km/s in these shots. The recovered sample of shot 787 is very well consolidated. The bonding between c-BN particles by the SCW texture is very sound. This sample is very hard and tough and the sample container was opened via surface grinding. The silicon carbide grinding wheel sparked brilliantly whenever it contacted the sample. A tungsten carbide probe deposited material onto the sample surface rather than scratching the sample. These observations are compatible with our previous shock compaction results

TABLE III. Cubic boron nitride (c-BN) plus SiC powder shock consolidation experiments.

Shot no.	Mass fraction (%) c-BN	Mass fraction (%) SiC	Initial density (%)	Flyer velocity (km/s)	Recovered results
980	80	20	70	1.89	Friable
982	80	20	60	1.96	Hard, many cracks
983	75 (diamond)	25	60	2.0	Recovered a small friable piece
1001	80	20	70	1.76	Still powder
1002	75	25	70	1.56	Still powder
1003	75	25	70	2.03	Friable

TABLE IV. Diamond plus silicon carbide whisker (SCW) sandwiched with Ti + C, shock consolidation experiments.

Experiments

Shot no.	Mass fraction (%) *Diamond*	Mass fraction (%) *SCW*	Initial *density (%)*	Flyer velocity (km/s)	*Recovered results*
766	80	20	60	1.30	Hard, large sample recovered with a few cracks
767	80	20	60	1.42	Same

Calculations

Shot no.	Initial density (%) Diamond	Initial density (%) SCW	P_H (GPa)	T_H (K) Diamond	T_H (K) SCW	T_p (K) Diamond	T_p (K) SCW	L (%) Diamond	L (%) SCW
766	63.7	49.7	10.5	965	1815	956	1793	5.0	20.9
767	63.7	49.7	11.6	1013	1963	1007	1936	5.6	23.0

of non-sandwiched c-BN plus SCW mixture performed with a 20 mm gun, in which a higher impact velocity (1.95 km/s) and initial density (~70% of crystal density) were used. Micro-Vickers hardness test shows the sample has a hardness of about 27 GPa. We also measured the sample's density and its longitudinal wave velocity. The results are given in Table VI. It appears that this sample achieved the crystal density of the mixture within the stated uncertainties.

In comparison with shot 787, the recovered sample of shot 786 shows a relatively lower hardness and less consolidation, due to the lower impact velocity. We thus

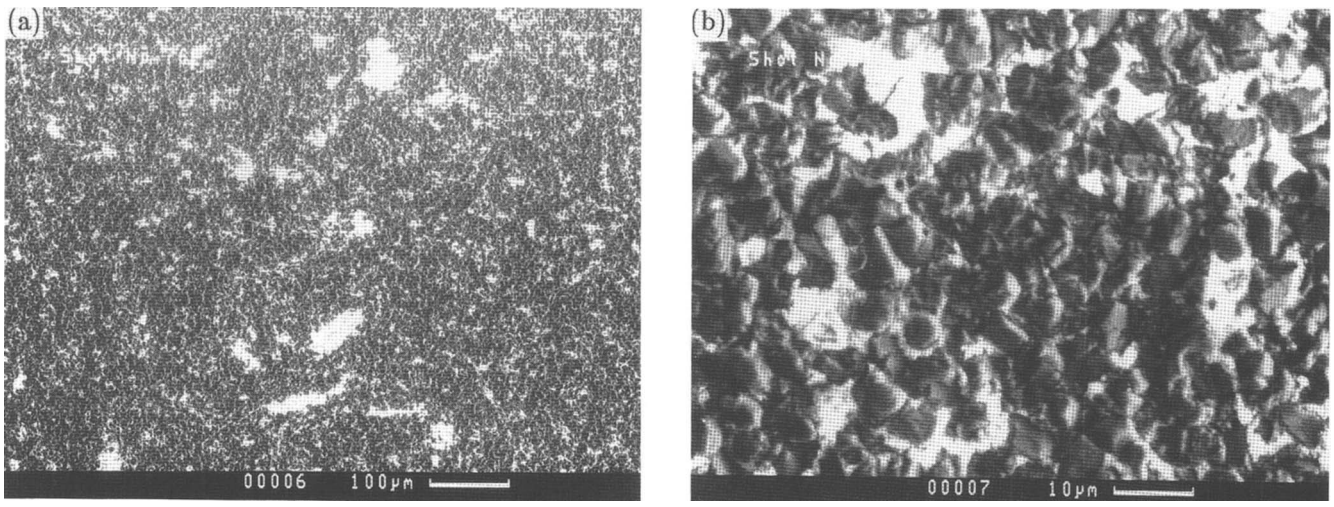

FIG. 4. SEM images of diamond plus SCW sandwiched with Ti + C. (a) and (b) show the cracks in the SCW-rich regions and the heavily pulverized diamond grains in the SCW deficient region of shot 767.

TABLE V. Shock consolidation results, c-BN plus SCW sandwiched with Ti + C.

Experiments

Shot no.	Mass fraction (%) c-BN	Mass fraction (%) SCW	Initial density (%)	Flyer velocity (km/s)	Recovered results
786	75	25	60	1.35	Hardness ~ hardened steel, few cracks
787	75	25	60	1.45	Hardness ~ harder than WC, few cracks
808[a]	75	25	60	1.36	Unconsolidated

Calculations

Shot no.	Initial density (%) c-BN	Initial density (%) SCW	P_H (GPa)	T_H (K) c-BN	T_H (K) SCW	T_p (K) c-BN	T_p (K) SCW	L (%) c-BN	L (%) SCW
786	66.7	47.0	10.3	919	1940	910	1920	5.1	22.8
787	66.7	47.0	11.6	977	2133	967	2109	5.8	25.7

[a]Not sandwiched with Ti + C.

expect better consolidation with a slightly higher velocity. Radial cracks still exist in the recovered samples, which are caused by the radial stress from the side rarefaction wave after shock wave passage. We believe these cracks can be eliminated by the use of appropriate radial momentum trapping.[10] Moreover, the use of star-shaped flyer plates as proposed by Kumar and Clifton[32] appears to be an effective tool for reducing cracking.[33] Also the use of impedance matching container[34] appears promising.

A SEM image is shown in Fig. 5 that demonstrates sound bonding between c-BN particles. Notably, no cracks can be seen in the c-BN crystals. This implies the c-BN single crystals are stronger than the man-made single crystal diamond upon shock consolidation.

F. Attempted shock compaction of SCW

Three experiments were conducted. Two of these totally failed. A third shot (shot 1004) was carried out without an Al_2O_3 shim at the impact end of the sample (Table VII).

SEM analysis of a small aliquot sample shows that these whisker materials are not compacted, and many of them still retain their original texture (Fig. 6). Calculations employing the shock wave data in Ref. 20 show that, with an impact velocity of 1.95 km/s, the initial shock pressure for shot 1004 is about 13 GPa. This pressure may be below the Hugoniot elastic limit of SCW. Only a very small amount of deformed sample material was found in the outer part of the recovered sample.

G. Diamond plus Si powder

Five experiments were conducted (Table VIII). All of them were recovered and very hard samples were obtained. The resulting samples can scratch glass or single crystal Al_2O_3. Samples obtained from high velocity (~2.0 km/s) impacts have micro-Vickers hardnesses up to 28 GPa. A typical SEM image (Fig. 7) demonstrates that all the Si powders are shock melted. Very sound bonding between diamond crystals by melted Si can be seen. As in other experiments with synthetic diamond powders, the diamond crystals are pulverized by shock loading. Shot 807 was performed with the 40 mm gun and sandwiched by Ti plus carbon black. The impact velocity is much lower (1.18 km/s) compared with other shots.

TABLE VI. Elastic moduli of superhard materials.

Crystal (structure)	Bulk modulus (GPa)	Shear modulus (GPa)	Density (g/cm^3)	Longitudinal wave velocity (km/s)
C (diamond)	441	532	3.51	18.1
BN-(diamond)	369	445	3.489	16.6
SiC (zincblende)	200	173	3.122	11.8
(Theoretical) 4 : BN + 1 : SiC	276	342	3.39	14.7
(Observed) 4 : BN + 1 : SiC			3.449 ± 0.19	12.27 ± 0.58

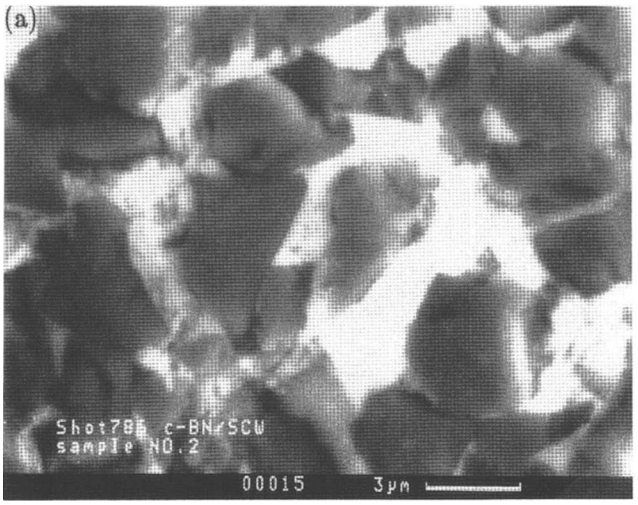

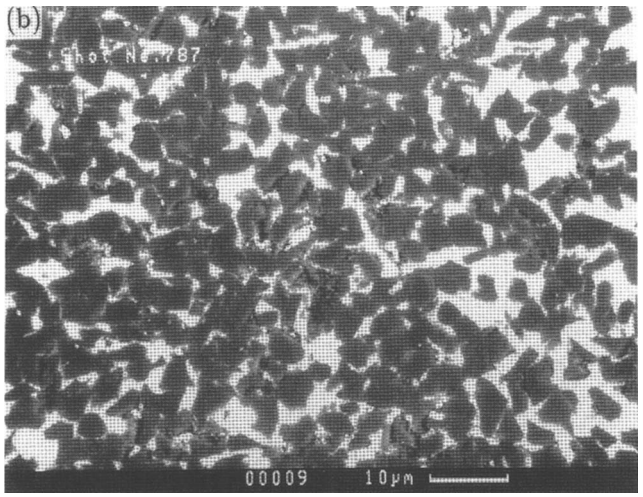

FIG. 5. SEM images of c-BN plus SCW sandwiched with Ti + C. (a) Shot 786; (b) shows very nice texture of SCW in shot 787. Note that no cracks can be seen in the c-BN grains.

IV. TEM RESULTS

The major objective of the TEM study of the present samples was to determine whether the SiC whisker and powder and/or diamond had melted along the interfaces, and whether diamond-silicon carbide reactions had occurred at the interface between phases. We also expected to determine whether cracks were present between phases, and in which phase shock induced cracks occurred.

TABLE VII. Attempted consolidation of SCW.

Shot no.	Initial density (%)	Flyer velocity (km/s)	Recovered results
998	60	1.95	Recovery capsule disintegrated
1000	61	1.75	Same
1004	60	1.95	Small aliquot recovered

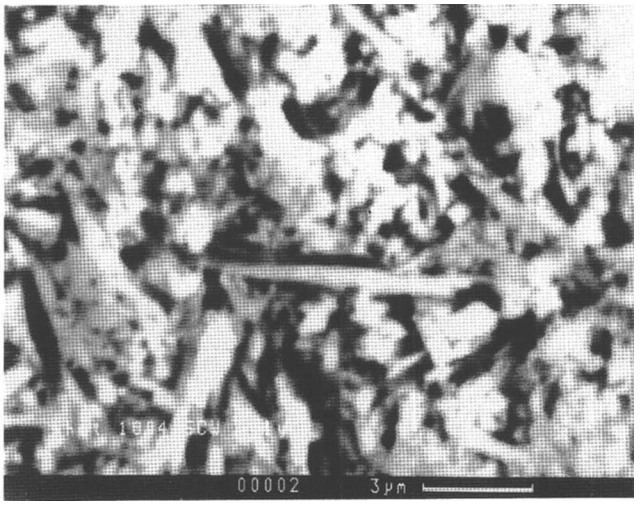

FIG. 6. Many SCW retain their original form after a 13 GPa shock compression (shot 1004).

Diamond samples consolidated with both SiC powder and SCW were sliced (to 0.5 mm thick) and then polished via a two-step abrasion with diamond paste to reduce their thickness down to 70–200 μm. After polishing, the samples were ion milled for ~100 h down to electron transparency (~10–100 nm) thick in a Commonwealth Scientific STATMMI-2 argon-ion milling apparatus. The temperature rise from room temperature was ~200 °C during ion thinning. These foils were in turn examined in a 100 keV JEOL Model 100C TEM. The question of possible dislocation motion in the course of ion-milling for 100 h at ~500 K was examined. Assuming a vacancy formation and migration model in which the self-diffusion activation energy is estimated to be ~7 eV, the diffusional losses of dislocations are calculated to be negligible for post-shock heating of 3000 K for 10 ms or during ion milling.

Both bright-field [Fig. 8(a)] and dark-field images [Figs. 8(c) and 8(d)] of the diamond admixed with the initially 0.28 μm β–SiC powder from shot 983 (see Table III) demonstrate that the SiC has completely recrystallized. Although a few grains appear to be as large as ~100 nm (0.1 μm) virtually all the single crystal domains are now in the size range of 30 nm or smaller, and the crystal orientation of the recrystallized SiC appears to be truly random. Moreover, the boundaries between what we assume to be recrystallized β–SiC and the diamond are smooth and in several cases are straight, indicating that interpenetrative motion between the diamond and SiC phase has been minimal. We infer that the diamond phase has not melted and recrystallized. There are no indications of reaction or solid solution between the diamond and SiC phases.

TABLE VIII. Shock consolidation of diamond plus Si powder.

Shot no.	Mass fraction (%)		Initial density (%)	Flyer velocity (km/s)	Recovered results
	Diamond	Si			
807[a]	95	5	60	1.18	Hard, scratches glass
1024	95	5	60	1.94	Harder than 807, scratches Al_2O_3
1026	90	10	60	2.01	Same
1027	95	5	60	1.90	Same
1031	95	5	60	2.0	Same

[a]Sandwiched with Ti + C.

The texture of the consolidated diamond plus SCW (Figs. 9 and 10) can be seen to be somewhat different. In Fig. 10 we again see the diamond surrounded by recrystallized SiC. However, the boundaries between the diamond crystal and the SiC are less smooth than in Fig. 8, for which the SiC started out as powder rather than whisker. The diamond is not heavily deformed in the sample from this experiment and, upon tilting the TEM stage, demonstrates a clear and consistent lack of the presence of dislocations. Thus we infer that the diamond phase undergoes only elastic deformation and brittle failure. The thermal history of the material (see below) makes it unlikely that the absence of dislocations is due to annealing. The crystal habit of the SiC material which started out as whisker can be seen to be completely different in the dark-field images [Figs. 9(c) and 9(d)] versus the sample where it started out as powder [Figs. 8(c) and 8(d)]. The SCW material has recrystallized into a series of quasilinear and coherent crystal bundles. Their dimensions are on the order of ~50 by 150 nm. Moreover, some open cracks ~200 nm long and 10–20 nm wide can be observed to terminate these bundles in Fig. 9(a). We think these microcracks are due to the volume contraction during consolidation. The deformation features in the diamond itself are well demonstrated in Fig. 11. Just like the SEM observations, the TEM images reveal that extensive brittle (presumably crystallographically controlled) cracking is present within individual diamond grains. Moreover, the crystal boundaries are not seriously deformed. The dark-field image [Fig. 11(b)] and the corresponding diffraction pattern [Fig. 11(c)] indicate that a moderate degree of streaking of the diffraction spots and microcrystalline rotation have occurred, and 100–300 nm regions of the crystal have been rotated via brittle shear strains. This microcrystalline rotation is not attributed to plastic deformation followed by annealing to give dislocation-free subgrains, because of the thermal history of the sample. The sample was shocked up to about 1000 K (see Table IV) by a shock wave with duration of about 1.5 μs. After the shock, it was heated up to about 3000 K by post-shock heating within a few milliseconds (see Sec. VI) and then cooled down to ambient temperature in approximately the same time interval. Thus, as discussed above, there was not enough time at high enough temperature for the dislocations to distribute themselves entirely into subboundaries.

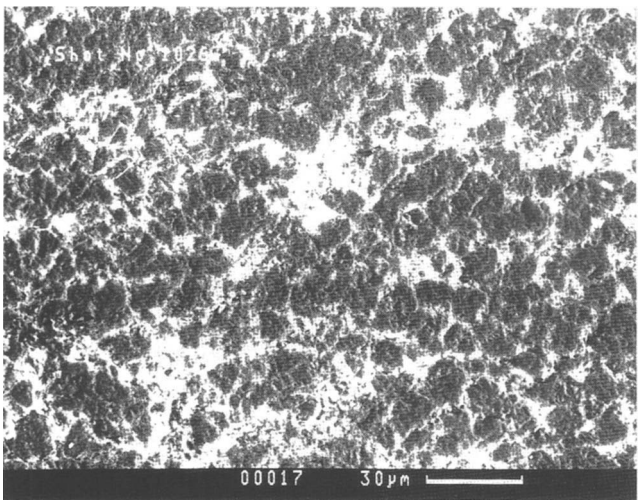

FIG. 7. SEM image of diamond plus Si powder in shot 1026. Completely melted Si gives the diamond grains a good bonding and all the diamond grains are fractured under shock loading.

We conclude from the TEM images that very little of the consolidation observed in the diamond-SiC system resulted from diamond grain boundary melting. The consolidated samples contain diamond held together with extensively melted and recrystallized β–SiC; there is no evidence to suggest plastic deformation of the diamond. The bundle fiber texture of the soundly consolidated material obtained with the recrystallized SCW versus the equant texture resulting from the melted recrystallized SiC powder gives rise to a marked difference in the resulting sample. The formation of equant microcrystallites implies that many crystal seeds were formed at the same time in the melted SiC and the SiC powder material achieved a lower temperature compared with the SCW which formed bundle-like crystallites.[12] The TEM and SEM analyses indicate that we need a thermo-

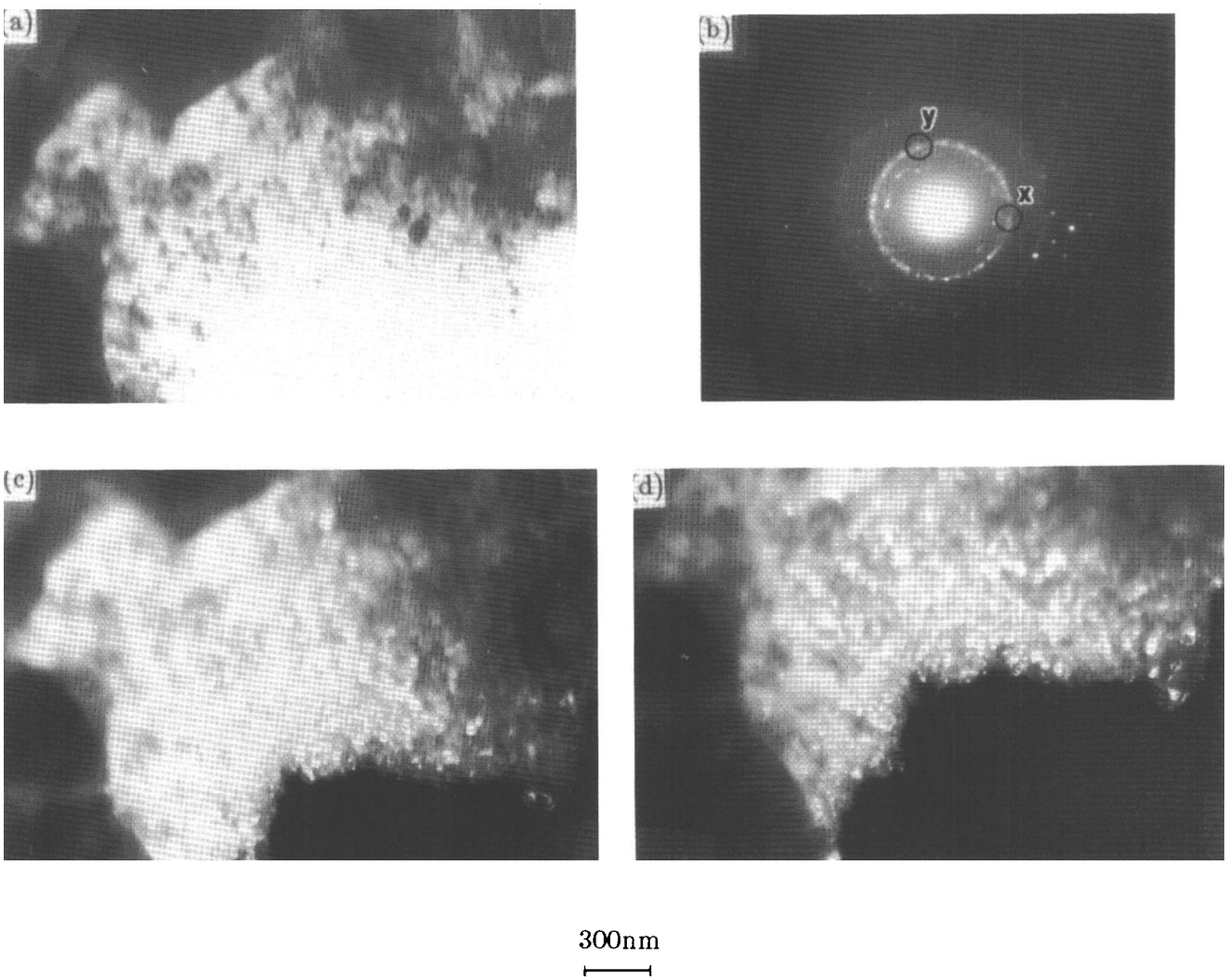

FIG. 8. TEM image of shot 983. Bright-field image (a) and diffraction pattern (b) of region of submicron SiC crystals; dark-field images, (c) and (d), taken for regions x and y of the diffraction pattern.

dynamic model that predicts, especially for the whiskers, virtually complete shock-induced melting of the SiC and no plastic deformation or significant melting of the diamond.

V. A NEW CALCULATION MODEL

Previously, in describing the thermodynamics of shock consolidation of superhard materials admixed with whiskers,[7] we employed a rather standard continuum approach. We assumed the hard power material and the whisker material could be described as having the same initial porosity. We also assumed that, upon shock loading, each phase was driven to an equal shock pressure along its individual porous Hugoniot. Our present observations, however, indicate that more melting occurs in the whisker material than is calculated from this previous model. Allowance must be made for the somewhat lower (ambient) melting points of SiC (2963 K) and Si_3N_4 (2173 K) as compared to diamond (4300 K) and c-BN (3273 K) as well as for the greater compressibility of SiC or Si_3N_4 (see Ref. 7, Figs. 3 and 5). As described in the previous sections, however, the contrast in melting behavior, especially for the admixtures with whiskers, appears to be considerably greater than would be expected on this basis alone. We think that in the vicinity of whiskers in the mixture, a larger effective porosity exists than in the coexisting powders. Thus the whisker material will have more space in which to achieve a locally higher compressional energy deposit, which is inferred to result in excess melting of the whiskers during shock consolidation, than the powder material.

In order to get the excess porosity of the essentially rod-like whiskers admixtured with approximately cube-shaped crystals, some packing information is needed. Milewski[13,31] did systematic packing experiments of sphere-rod mixtures. It turns out that the distension, M,

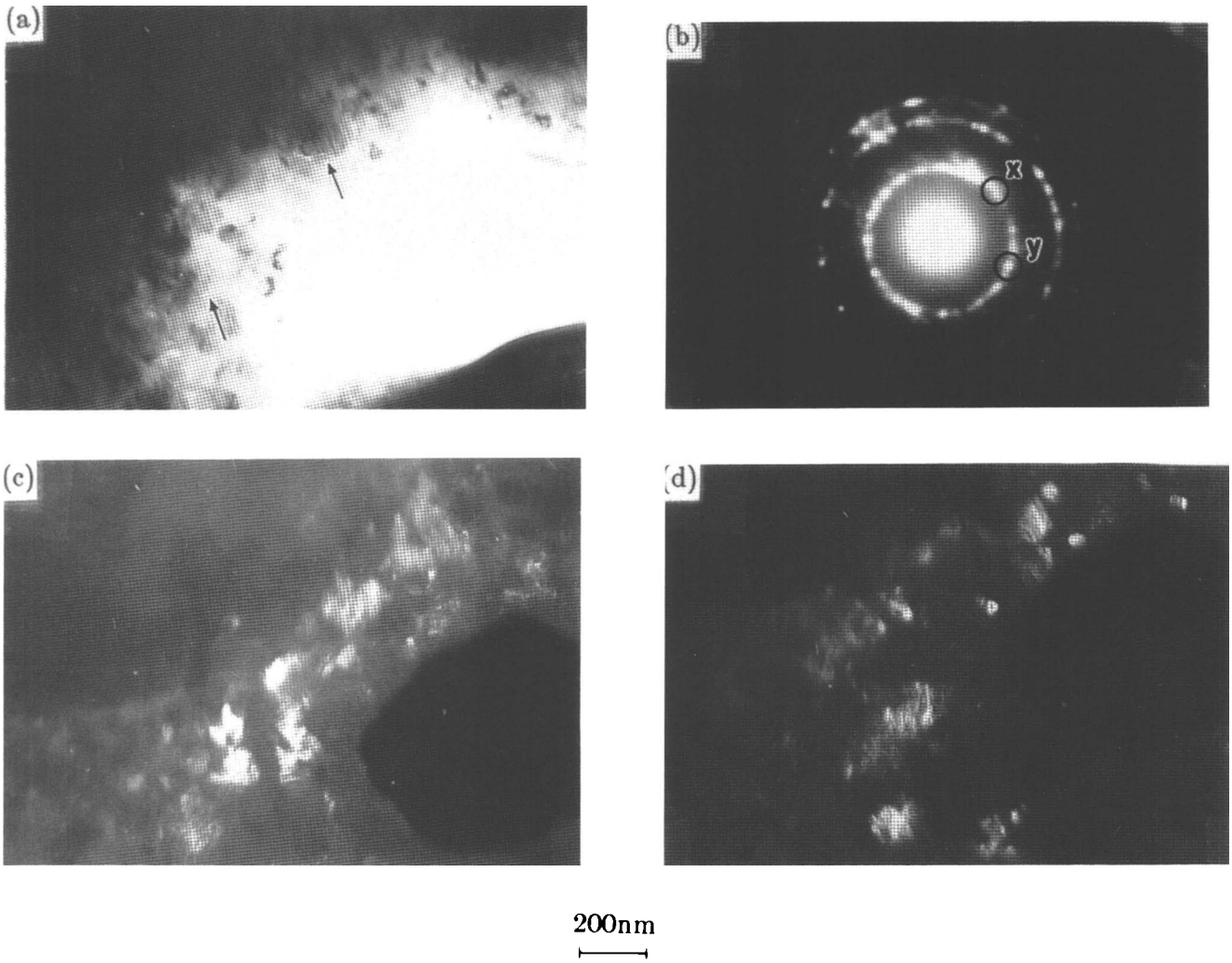

FIG. 9. TEM image of shot 973. Bright-field image (a) and diffraction pattern (b) of region of submicron SiC crystals observed between diamond single crystals; dark-field images, (c) and (d), taken for regions x and y of the diffraction pattern. Arrows in (a) indicate small cracks.

of the mixture is a function of the length to diameter ratio, L/D_r, of the rods, the diameter ratio, D_s/D_r, of spheres to rods, and the solid volume fraction (without porosity), F, of the rods. M is defined as the ratio of the volume with porosity divided by the pore-free volume. In our consolidation experiments, the average L/D_s is about 50, average D_s/D_r is about 3 to 4, and F ranges from about 0.1 to 0.4. Packing data with $D_s/D_r = 1.95$, 3.71, 6.97, 14.32, and 17.4 are obtained by Milewski. The data with $D_s/D_r = 3.71$ are used. Figure 12 shows the data with $D_s/D_r = 3.71$ and some experimental points we conducted for $D_s/D_r = 3$. The vertical axis is distension of the mixture, and the axis of abscissa is the length to diameter ratio of whiskers. Unfortunately, there are no data for L/D_r equal to 50, which we need. Hence, we simply fit the data and extrapolate them to $L/D_r = 50$. In fitting the data, we made an assumption that if F and D_s/D_r are constant, when L becomes very large, M equals the distension with no rods, $M_0 = 1.624$. This assumption is reasonable in considering the geometry of the mixture. That is, when the rods become longer, the number density of the rods will decrease and the excess porosity generated will decrease and thus the distension will decrease.

The distension M at $L/D_r = 50$ for different F were fitted as

$$M = 1.552 + 0.03279 \exp(7.633F) \quad (0.1 < F < 0.4) \quad (1)$$

So, we have

$$(M - M_0)/M_0 = -0.04433 + 0.0202 \exp(7.633F) \quad (0.1 < F < 0.4) \quad (2)$$

where $M - M_0$ is the distension increase because of the addition of rods, ΔM.

Assuming that in our sample, the distension increase and the distension of pure crystal have the same relation

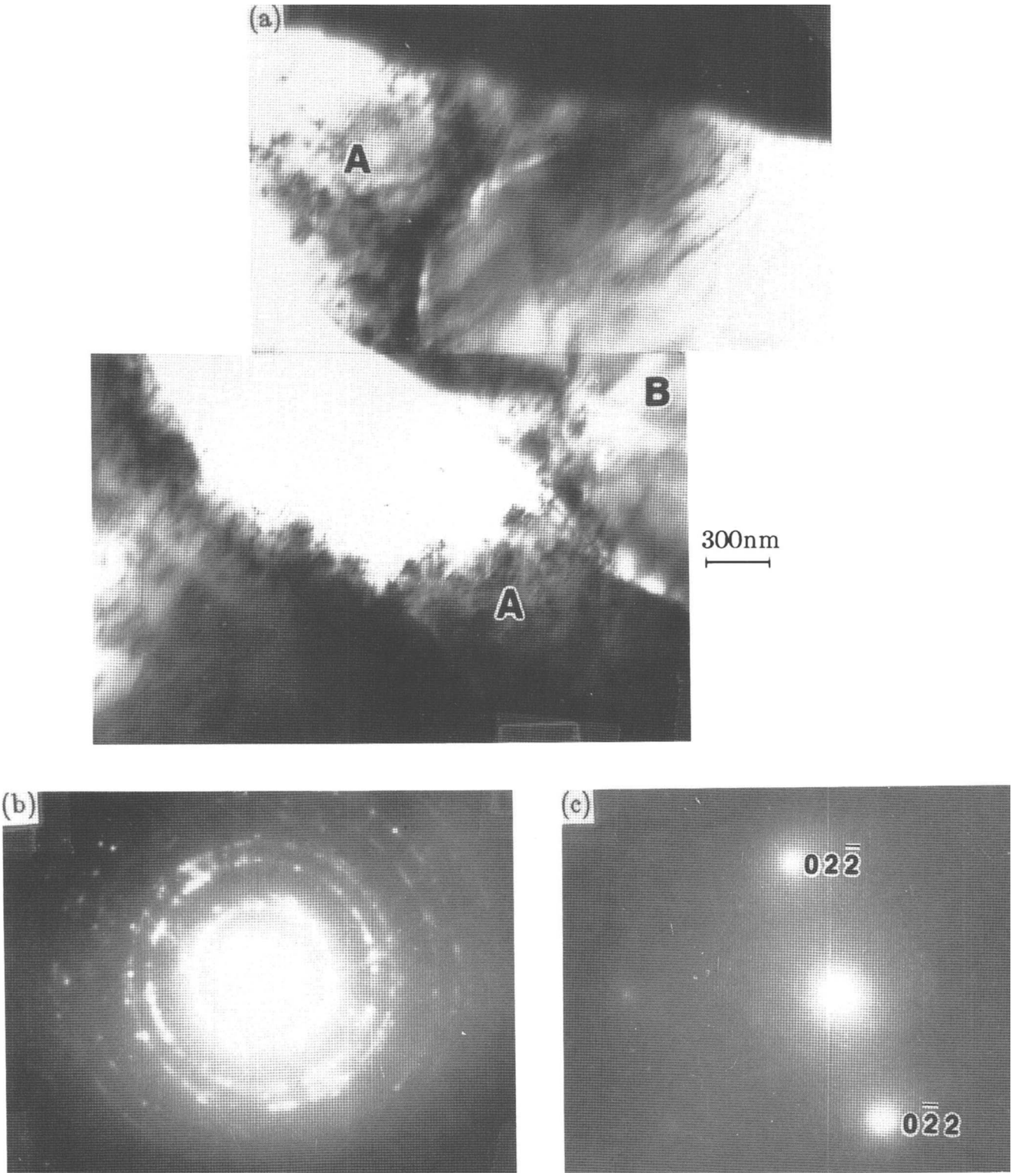

FIG. 10. TEM image of shot 973. (a) Montage showing regions of small SiC crystals (A) surrounding diamond single crystal (B); (b) and (c) diffraction patterns from regions (A) (lower) and (B), respectively.

as shown in Eq. (2), plus the distension conservation condition of the mixture

$$M = M_0 + \Delta M \qquad (3)$$

we can calculate the distension of crystals, M_0, and the distension increase because of the addition of whiskers, ΔM. Designating ΔM to whiskers only, we get the bulk densities of crystals and whiskers, respectively. For

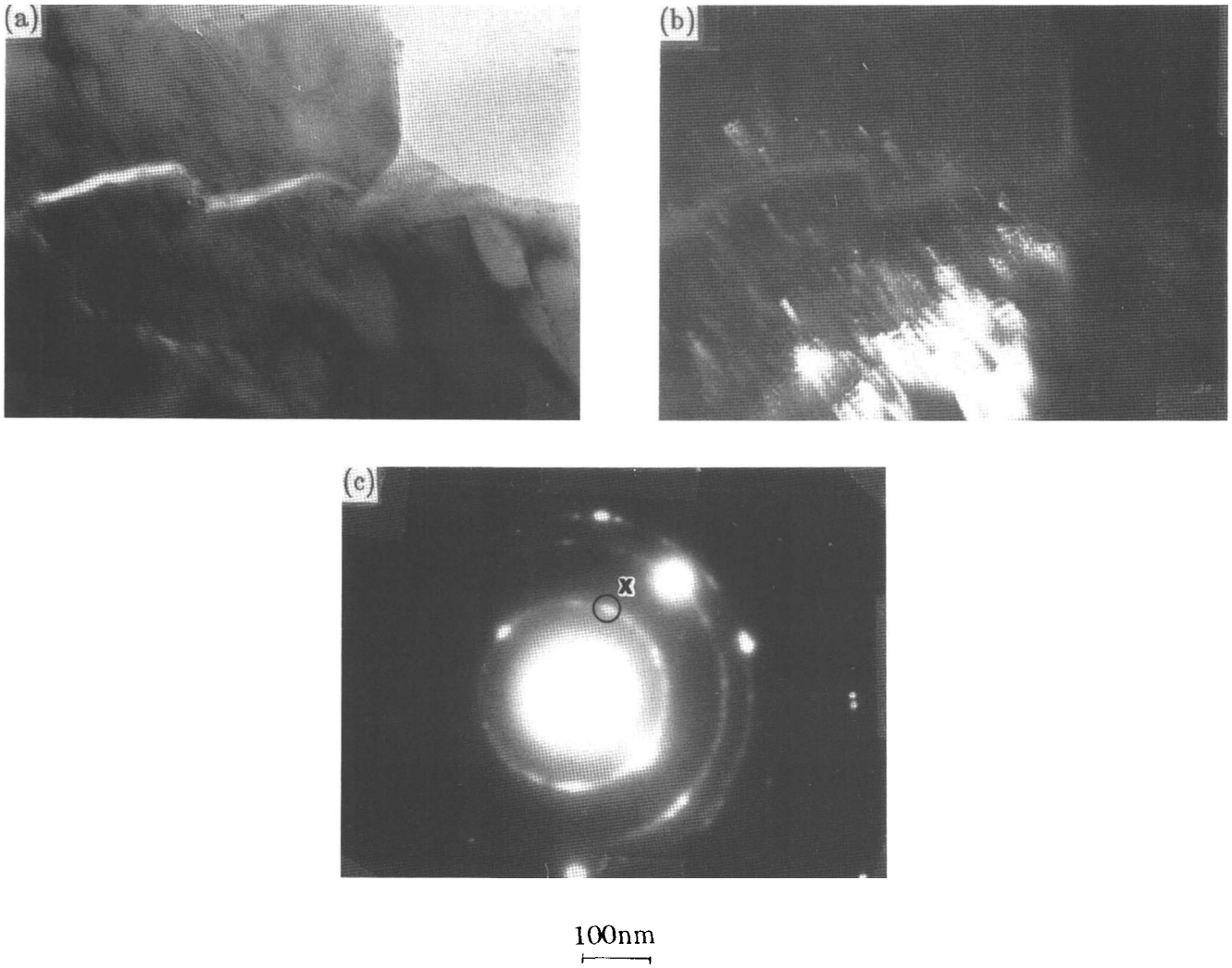

FIG. 11. TEM image of shot 767. Bright-field (a) and dark-field (b) images and diffraction pattern (c) of diamond region showing small crystals and cracking. Dark-field image taken for region x in diffraction pattern.

example, in shot 953 (Table I), with $M = 1.538$ and $F = 0.174$, we get $M_0 = 1.491$ and $\Delta M = 0.047$; the bulk densities of diamond and SNW are 67.1% and 56.8% of their crystal densities, respectively.

After the initial densities of powders and whiskers in the admixture were obtained by the procedure outlined above, a series of thermodynamic calculations were conducted. Shock pressure, P_H, temperature, T_H, post-shock temperature, T_p, and percent of material melted, L, were calculated. The results are presented in Tables I-II, IV-V, and IX-X. The assumptions in the calculation are the same as before[7] except that the powders and whiskers have different initial densities. Details of the calculations are presented in the appendix. The parameters used are listed in Table XI. Table IX and Table X give the results of the revised calculations for the experiments described in Ref. 7. The new calculation predicts much higher shock temperatures and more melting of the whisker materials SNW and SCW. For example, for shot 936 (Table IX), the new calculation yields 73.3% melt and a shock temperature of 2173 K (melting point) of SNW, whereas the previous one yields only 48.8% melt and 1876 K. We believe that, at such high temperatures (near or at the melting point), the whisker material will lose its strength completely and change shape, either plastically or by fluid flow, to form the observed texture in the recovered sample. In contrast, the diamond and c-BN powders achieve relatively low temperatures compared with their melting points and are therefore neither plastically deformed nor extensively melted.

VI. POST-SHOCK HEATING WITH Ti + C

The concept of post-shock heating was first suggested by Sawaoka and Akashi.[8] The reason we use titanium plus carbon as a heat source is that the reaction

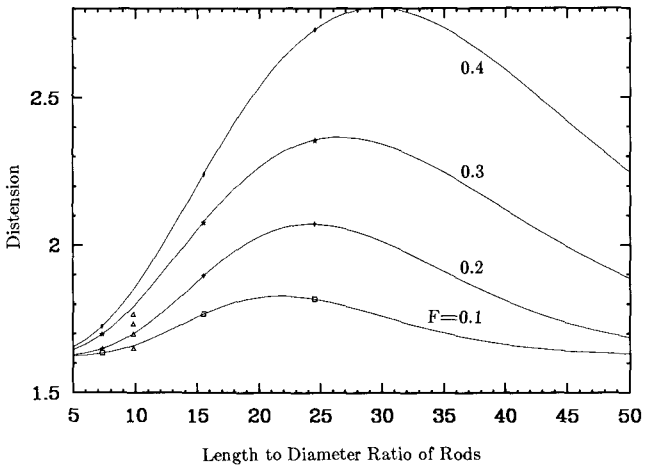

FIG. 12. Distension of sphere rod mixture versus length to diameter ratio of rods. The data points are Milewski's data[31] for $D_s/D_r = 3.71$. The solid lines are fitted lines at different solid volume fraction, F, of rods. The triangle symbols are our packing results with $D_s/D_r = 3$.

has a large reaction heat[17] ($\Delta H = 3037$ J/g) and the titanium and carbon can react completely with each other under shock compression.[8] Fe_2O_3 plus Al may also be a good candidate for post-shock heating (its reaction heat is about 4000 J/g when completely reacted), but Boslough has studied this reaction under shock-wave loading and pointed out that reaction under shock may be incomplete.[22]

The Ti powder we used has a size range of 1–3 μm and is mixed with carbon black in a stoichiometric ratio. The reaction equation is

$$\mathrm{Ti} + \mathrm{C} = \mathrm{TiC}$$

If T is the post-shock temperature of the product TiC, the energy balance equation is

$$\Delta H + E_H = \int_{300}^{T} C_p \, dT + L\Delta H_m \tag{4}$$

where E_H is the Hugoniot energy, C_p is the specific heat of TiC,[17] L is the melting fraction of TiC, and the latent heat ΔH_m of melting of TiC is 1187 J/g.[17] The Hugoniot energy is dependent on the shock pressure and the initial state of Ti + C. If the crystal specific volume V_{0c} of TiC is used as an approximation of the Hugoniot specific volume, then E_H is given approximately as

$$E_H = \frac{1}{2} P_H (V_{00} - V_{0c}) \tag{5}$$

where V_{00} is the initial specific volume of Ti + C, and V_{0c} equals 0.2025 cm^3/g.[17] The appendix describes how the Ti + C Hugoniot is derived.

If ϕ is the initial fractional porosity, E_H can be expressed as

$$E_H = \frac{1}{2} P_H V_{0c} \frac{\phi}{1-\phi} \tag{6}$$

With Eqs. (4) and (6), we get the $T - P_H$ relation at different values of ϕ. For example, for $\phi = 40\%$, the reaction heat itself will heat the TiC to its melting point (3293 K) and melt 48.5% of it when $P_H = 0$; when $P_H = 9.05$ GPa, the TiC will be completely melted. Some calculational results are illustrated in Fig. 13. It is clear that the higher the pressure or the greater the initial porosity, the higher the post-shock temperature that the TiC will reach; that is, more heat will be released from TiC.

TABLE IX. Revised calculation results for c-BN plus SNW shock consolidation experiments.

Experiments

Shot no.	Mass fraction (%) c-BN	Mass fraction (%) SNW	Initial density (%)	Flyer velocity (km/s)	Recovered results
932	85	15	60	1.95	Consolidated
936	85	15	71	1.94	Well consolidated

Calculations

Shot no.	Initial density (%) c-BN	Initial density (%) SNW	P_H (GPa)	T_H (K) c-BN	T_H (K) SNW	T_p (K) c-BN	T_p (K) SNW	L (%) c-BN	L (%) SNW
932	61.5	53.2	20.0	1530	2173	1508	2173	12.5	85.4
				1154[a]	2081[a]			11.3[a]	55.4[a]
936	72.8	63	25.7	1314	2173	1279	2173	9.5	73.3
				929[a]	1876[a]			8.8[a]	48.8[a]

[a]Results from Ref. 7.

TABLE X. Revised calculation results for c-BN plus SCW shock consolidation experiments.

Experiments

Shot no.	Mass fraction (%) c-BN	Mass fraction (%) SCW	Initial density (%)	Flyer velocity (km/s)	Recovered results
937	85	15	71	2.01	Uncompacted
938	80	20	70	1.95	Consolidated
939	75	25	71	1.97	Consolidated, friable

Calculations

Shot no.	Initial density (%) c-BN	Initial density (%) SCW	P_H (GPa)	T_H (K) c-BN	T_H (K) SCW	T_p (K) c-BN	T_p (K) SCW	L (%) c-BN	L (%) SCW
937	72.8	63.0	27.2	1362	2587	1324	2479	10.1	31.4
				968[a]	1972[a]			9.3[a]	19.7[a]
938	74.2	58.0	25.2	1245	2868	1213	2769	9.6	35.8
				937[a]	1834[a]			9.0[a]	19.2[a]
939	78.9	55.7	26.1	1101	2963	1067	2963	6.9	40.8
				895[a]	1845[a]			8.8[a]	18.9[a]

[a]Results from Ref. 7.

In the shock consolidation, the post-shock heating is probably very important, especially in the comparatively low pressure range. Successful shock compaction is probably impossible under low pressure without post-shock heating, for the following reasons. Under low pressure, very little melt can be obtained and this will not be sufficient to bond the particles together. The relatively low shock pressure also implies that the brittle particles will not be able to change their shape plastically to give a dense compact. In addition, the rapid cooling of the sample will induce cracks. In the case of post-shock heating via the Ti + C = TiC reaction, the sample is able to cool slowly and thus eliminate the formation of cracks due to rapid cooling, and remove residual stresses. The post-shock heating can also heal the cracks induced during the pressure release process and possibly also remove voids from the sample via conventional sintering action. Shot 808 (see Table V) was conducted without Ti + C. The flyer velocity is 1.36 km/s (almost the same as shot 786). The recovered sample is uncompacted. These two shots exemplify the importance of post-shock heating of the sample by TiC formation.

As an example, we calculated the time dependent temperature profiles of shot 766 (Table IV, Fig. 15) for the geometry shown in Fig. 14. We assumed that, after shock loading, the sample, TiC, and 304 stainless steel (S.S.304) capsule are each at their crystal density, and that the heat flow is one-dimensional. We chose a typical initial sample thickness of 2 mm, but varied the thickness of TiC from 0.25 to 1.0 mm corresponding to the thickness of Ti + C from 0.8 to 1.7 mm at porosity of 40%.

TABLE XI. Parameters.

	Diamond	c-BN	SCW	SNW
γ_0	0.9[14]	1.87[18]	1.25[20]	1.25[a]
C_0 (mm/μs)	12.16[14]	10.29[18]	8.0[20]	7.90[21]
S	1.00[14]	1.25[18]	0.95[20]	1.20[21]
ρ_0 (g/cm^3)	3.51[15]	3.487[15]	3.18[15]	3.18[15]
θ (K)	1600[16]	1900[16]	1140[20]	1067[b]
T_m (K)	4300[17]	3273[7]	2963[15]	2173[15]
H_m (kJ/g)	9.2[19]	9.2[19]	4.9[19]	1.081[c]

γ_0: Grüneisen coefficient; C_0 and S: constants in $D = C_0 + SU$; ρ_0: crystal density; θ: Debye temperature; T_m: melting point; H_m: latent heat of melting.

[a]SiC value.

[b]Derived from its specific heat at 298 K in Ref. 15.

[c]Estimated by assuming that it has the same entropy increase per mole upon melting as that of SiC.

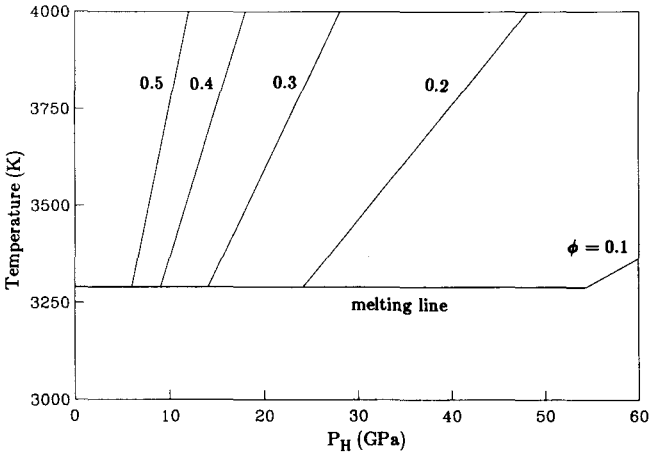

FIG. 13. Post-shock temperature of TiC versus shock pressure P_H at different initial porosity (ϕ). Melting line shown is appropriate for TiC.

To solve the one-dimensional heat equation, a finite differential numerical method was employed.[23] The thermal diffusivities used here are 4×10^{-6} m^2/s (S.S.304),[24] 10^{-4} m^2/s (diamond),[7] and 5×10^{-6} m^2/s (SCW).[7] For simplicity, a constant specific heat of 0.4 J/gK[24] was assumed for S.S.304. The Debye specific heat model was used for diamond (Debye temperature, 1860 K) (see Table XI) and SCW (Debye temperature, 1140 K) (see Table XI). To simplify the calculation further, we chose the thermal diffusivity of TiC as infinite. The post-shock temperature rise of S.S.304 was omitted, for it is small.[20] The calculation results are shown in Fig. 15. Calculations were performed for four different thicknesses of TiC. We can see from Fig. 15 that a thicker TiC layer gives the sample a higher average temperature. In Fig. 15(d), an average temperature of 3000 K [higher than the melting point (2963 K) of SCW] was obtained and the SCW in the sample must be melted in this case. In Fig. 15(b), with a TiC thickness of 0.5 mm, which corresponds to 0.83 mm porous Ti + C, the average temperature of the sample reached 2370 K, which is 80% of the melting point of SCW. It is known that the carbides will lose their brittleness at a temperature 80–90% of their melting points.[25] So we infer that SCW will be efficiently annealed in this case. The optimum thickness for this proposed process is approximately 0.8 to 1.7 mm when the initial porosity of Ti + C is 40%, under a shock pressure of 10 GPa which is typical of these experiments. The porous Ti + C thicknesses we used in the present experiments were 0.8–1.5 mm, which are very close to what we infer is optimum from the calculations.

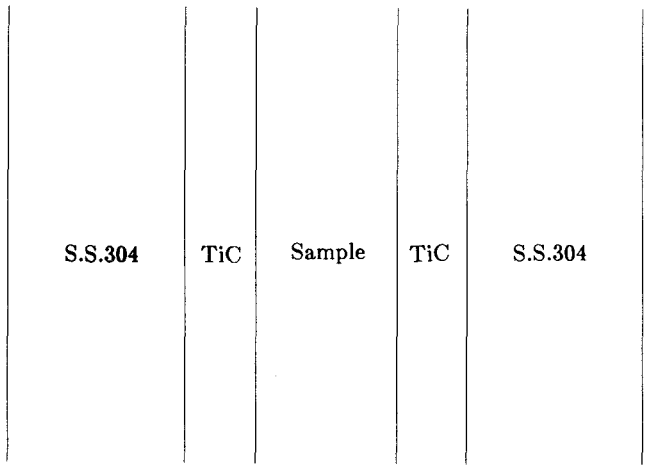

FIG. 14. Geometry assumed in calculation of post-shock heating.

VII. DISCUSSION AND CONCLUSION

The shock wave consolidation mechanism in an admixture of a superhard powder and a whisker material is the melting and recrystallizing of the whisker material. Rod-like whiskers have a higher effective porosity as compared with the average environment of cube-shaped crystals in the mixture. Whisker deformation and melting are enhanced by this excess space. We note that the whisker materials have lower melting temperature and strength as compared with diamond or c-BN powder. In contrast, when fine SiC powder is admixed with sphere-like diamond or c-BN powder, it fills the voids between the particles and no excess space can be obtained. Thus the fine SiC powder results in lower post-shock temperatures upon shock consolidation and therefore is not suitable as an additive material. Our new calculation model of powder plus whisker provides a physically based explanation of the experimental results.

The effect of post-shock heating obtained from the reaction Ti + C = TiC is important in consolidation under low dynamic pressure. Very well consolidated samples composed of c-BN plus SCW were obtained with the post-shock heating technique for shock compaction at a pressure of 12 GPa.

Brittle failure of synthetic diamond crystals during shock loading occurred in most of our experiments. In comparison, c-BN single crystals appear to be unaffected by shock loading when admixed with whisker material.

The SNW material, because of its reaction with carbon under higher temperature and pressure, is not suitable for shock compaction when mixed with diamond powder; the SCW yields better compacts.

The commercially obtained Si powder (<44 μm) shows some promise as a beneficial additive in consolidation of diamond. Well-consolidated diamond samples were obtained with 5% or 10% Si. Further work needs to be conducted in this area.

It appears, at present, that c-BN plus SCW is the most promising material to obtain practically

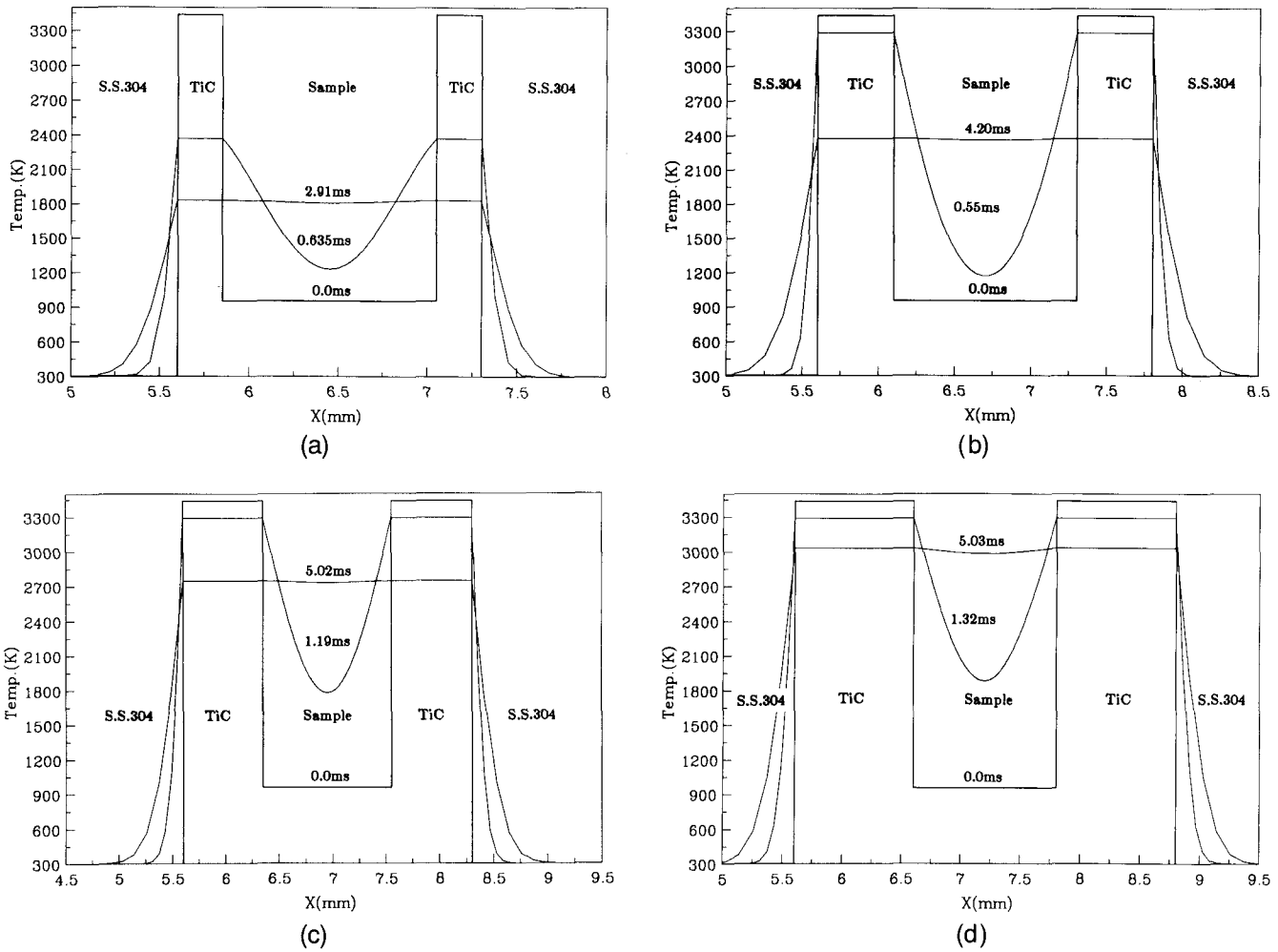

FIG. 15. Calculated temperature profiles of post-shock heating. (a) The thickness of TiC is 0.25 mm, and the average temperature of the sample reaches 1819 K at 2.91 ms; (b) TiC 0.5 mm thick, average temperature 2370 K at 4.20 ms; (c) TiC 0.75 thick, average temperature 2737 K at 5.02 ms; (d) TiC 1.0 mm thick, average temperature 3000 K at 5.03 ms.

useful superhard polycrystalline compacts via shock consolidation.

ACKNOWLEDGMENTS

This research was supported by California Institute of Technology, New Mexico Institute of Mining and Technology, and United States Army Research Office Contract No. DAAL03-88-K-0199, contribution number 4869, Division of Geological and Planetary Sciences.

REFERENCES

1. D.K. Potter and T.J. Ahrens, Appl. Phys. Lett. **51**, 317–319 (1987).
2. F.P. Bundy and R.H. Wentorf, J. Chem. Phys. **38**, 1144–1149 (1963).
3. T. Akashi, V. Lotrich, A. Sawaoka, and E.K. Beauchamp, J. Am. Ceram. Soc. **68**, c-322–c-324 (1985).
4. T.J. Ahrens and D.K. Potter, in *Shock Waves in Condensed Matter–1987*, edited by S.C. Schmidt and N.C. Holmes (North-Holland Physics Publishing, Amsterdam, The Netherlands, 1988), pp. 419–422.
5. S. Sawai and K. Kondo, J. Am. Ceram. Soc. **71**, c-185–c-188 (1988).
6. T. Akashi and A.B. Sawaoka, J. Mater. Sci. **22**, 1127–1134 (1987).
7. H. Tan and T.J. Ahrens, J. Mater. Res. **3**, 1010–1020 (1988).
8. A. Sawaoka and T. Akashi, in *Shock Waves in Condensed Matter–1987*, edited by S.C. Schmidt and N.C. Holmes (North-Holland Physics Publishing, Amsterdam, The Netherlands, 1988), pp. 423–425.
9. JANAF Thermodynamical Tables, edited by M.W. Chase, Jr., C.A. Davies, J.R. Downey, Jr., D.J. Frurip, R.A. McDonald, and A.N. Syverud (American Chemical Society and the American Institute of Physics for the National Bureau of Standards, 1985), pp. 1563, 634.
10. G.T. Gray, Metall. Trans. **20A**, June, 1989.
11. *LASL Shock Hugoniot Data,* edited by S.P. Marsh (University of California, Berkeley, CA, 1980), pp. 328, 249.
12. R.W. Heine, C.R. Loper, Jr., and P.C. Rosenthal, *Principles of Metal Casting* (McGraw-Hill Book Company, New York, 1967), pp. 178–209.
13. *Handbook of Fillers and Reinforcements for Plastics,* edited by Harry S. Katz and John V. Milewski (Van Nostrand Reinhold Company, New York, 1978), p. 66.

14. M. N. Pavlovskii, Sov. Phys. Solid State **13**, 741–742 (1971).
15. Tateho Chemical Industries Co., Ltd., technical data, 1988.
16. T. Soma, A. Sawaoka, and S. Saito, in *Proc. Fourth Int. Conf. on High Pressure–1974*, Special Issue of the Rev. of Phys. Chem. Jpn., edited by J. Osugi (Kawakita, Kyoto, Japan, 1975), pp. 446–453.
17. *Lange's Handbook of Chemistry*, edited by J. A. Dean (McGraw-Hill, Inc., New York, 1985), p. 3-2, 9-63, 9-137, 4-123.
18. E. Knittle, R. M. Wentzcovitch, R. Jeanloz, and M. L. Cohen, Nature **337**, 349–352 (1989).
19. J. A. Van Vechten, Phys. Rev. B **7**, 1479–1507 (1973).
20. R. Kinslow, *High Velocity Impact Phenomena* (Academic Press, Inc., New York, 1970), p. 549, 551, 374.
21. Derived from T. Mashimo's data in *Shock Waves in Condensed Matter–1987*, edited by S. C. Schmidt and N. C. Holmes (North-Holland Physics Publishing, Amsterdam, The Netherlands, 1988), pp. 289–292.
22. M. B. Boslough, A Thermodynamical Model for Shock-Induced Chemical Reactions in Porous Solids: Analogs and Contrasts to Detonation, in Proc. 9th Symp. (Int.) on Detonation–1989.
23. J. M. Hill and J. N. Dewynne, *Heat Conduction* (Blackwell Scientific Publications, 1987), p. 197.
24. J. H. Lienhard, *A Heat Transfer Text Book* (Prentice-Hall, Inc., Englewood Cliffs, NJ, 1981), p. 492.
25. P. Schwarzkopf and R. Kieffer, *Cemented Carbides* (The Macmillan Company, New York, 1960), p. 67.
26. T. J. Ahrens, in *Methods of Experimental Physics* (Academic Press, New York, 1987), Vol. 24, Part A, pp. 185–234.
27. T. J. Ahrens, D. Kostka, P. Kasiraj, and T. Vreeland, Jr., in Rapid Solidification Processing Principles and Technologies, III, *Proc. 3rd Conf. on Rapid Solidification Processing*, edited by R. Mehrabian (U. S. National Bureau of Standards, Gaithersburg, MD, 1982), pp. 672–677.
28. W. H. Gourdin, J. Appl. Phys. **55**, 172–181 (1984).
29. R. B. Schwarz, P. Kasiraj. T. Vreeland, Jr., and T. J. Ahrens, Acta Metall. **32**, 1243 (1984).
30. R. A. Robie, B. S. Hemingway, and J. R. Fisher, Thermodynamic Properties of Minerals and Related Substances at 298.15 K and 1 bar (10^5 pascals) Pressure and at Higher Temperatures (Geological Survey Bulletin 1452, 1978), p. 41.
31. John V. Milewski, A Study of the Packing of Fibers and Spheres, Ph.D. Thesis, Rutgers University (1973).
32. P. Kumar and R. J. Clifton, J. Appl. Phys. **48**, 4850 (1977).
33. R. L. Rabie, J. E. Vorthman, and J. K. Dienes, *Shock Waves in Condensed Matter–1983*, edited by J R. Asay, R. A. Graham, and G. K. Straub (Elsevier Science Publisher B.V., 1984), pp. 199–202.
34. A. Mutz and T. Vreeland, Jr., Several Techniques for One-Dimensional Strain Consolidation of Multiple Cavities, in *Proc. Int. Conf. On High Strain Phenomena in Materials*, edited by L. E. Murr, M. Meyers, and K. P. Staudhammer (1991).

APPENDIX

A. Shock pressure P_H

The impedance match technique[26] was used to calculate the shock pressure in the sample from the measured flyer velocity and the sample Hugoniot estimated below.

From the Grüneisen equation of state, we can get the porous Hugoniot on the P-V plane (see Fig. A) as

$$P_H = \frac{P_d\left(\frac{V_{0d}-V_d}{2} - \frac{V_d}{\gamma}\right)}{\frac{V_{00}-V_d}{2} - \frac{V_d}{\gamma}} \qquad \text{(A1)}$$

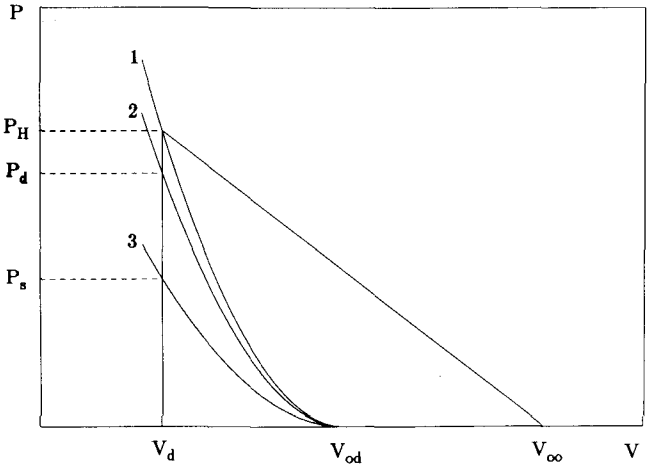

FIG. A. P-V plane. Curves 1, 2, and 3 are porous Hugoniot, known Hugoniot centered at V_{0d}, and adiabat, respectively.

in which V/γ = constant is assumed.

With the porous Hugoniot obtained from Eq. (A1), the mixture Hugoniot is obtained on the basis of volume additivity at constant pressure.[20]

For convenience of calculation of the shock pressure, we use the shock relations

$$U_s = V_{00}[P_H/(V_{00} - V_d)]^{1/2} \qquad \text{(A2)}$$

$$U_p = [P_H(V_{00} - V_d)]^{1/2} \qquad \text{(A3)}$$

to obtain the linear relation $U_s = C_0 + SU_p$ (Ref. 26).

The Hugoniot data used for c-BN, diamond, and SiC are from Refs. 11, 14, and 20, respectively.

B. Calculation of continuum shock temperature T_H

The continuum shock temperature T_H of each constituent is calculated by the method of Ref. 26.

$$\int_{T_s}^{T_H} C_v\, dT = E_H - E_s \qquad \text{(A4)}$$

where C_v is the Debye specific heat. The Hugoniot energy and isentropic energy are

$$E_H = \frac{1}{2}P_H(V_{00} - V) \qquad \text{(A5)}$$

$$E_s = -\int_{V_{0d}}^{V} P_s dV \qquad \text{(A6)}$$

The isentropic pressure P_s and temperature T_s are

$$P_s = -\rho_0 C_0^2 \exp(\gamma\eta) \int_0^\eta [(\gamma - S)x - 1] \Big/ \left[\exp(\gamma x)(1 - Sx)^3\right] dx \qquad \text{(A7)}$$

$$T_s = T_0 e^{\gamma\eta} \qquad \text{(A8)}$$

where $\eta = 1 - V/V_0$.

C. Calculation of the post-shock temperature T_p

Assuming each constituent release along its Hugoniot curve to V_{0d}, the post-shock temperature T_p is given by the following equations:

$$\int_{T_0}^{T_p} C_v \, dT = \frac{1}{2} P_H (V_{00} - V_H) - \int_{V_H}^{V_{0d}} P_H \, dV \quad \text{(A9)}$$

$$P_H = C_0^2 \eta \Big/ \left[V_{0d} (1 - S\eta)^2 \right] \quad \text{(A10)}$$

D. Melting fraction L

The formula used to calculate melt fraction is[27–29]

$$L \leqslant \frac{P_H (V_{00} - V_{0d})}{2[C_p (T_m - T_0) + H_m]} \quad \text{(A11)}$$

where C_p is the specific heat, and T_m and H_m are the melting point and latent heat of fusion, respectively.